Electromyographic Mapping of Finger Stiffness in Tripod Grasp: a Proof of Concept

Matteo Rossi, Alessandro Altobelli, Sasha B Godfrey, Arash Ajoudani and Antonio Bicchi

***Abstract*—Effective execution of a manipulation task using prosthetic or robotic hands requires that the motion and the impedance profiles of the fingers be appropriately commanded. This, however, brings some design and control challenges regarding the individual planning and realization of the finger motion and stiffness trajectories. It appears that the central nervous system solves for this complexity in an effective and coordinated manner which has been well-recognized under the concept of hand synergies. While the exploitation of this concept in kinematic coordinates has lead to the development of several successful robotic designs and control strategies, its extension to dynamic coordinates, such as coordinated stiffening of the fingers, remains to be investigated. Indeed, in this study we provide preliminary evidence on the existence of such coordinated stiffening patterns in human fingers and establish initial steps towards a real-time and effective modelling of the finger stiffness in a tripod grasp. To achieve this goal, the endpoint stiffness of the thumb, index and middle fingers of five healthy subjects are experimentally identified and correlated with the electromyography (EMG) signals recorded from a dominant antagonistic pair of the forearm muscles. Our findings suggest that: i) the magnitude of the stiffness ellipses at the fingertips grows in a coordinated way, subsequent to the co-contraction of the forearm muscles; ii) the length of the ellipses' axes appears to have a nearly linear relationship with the co-contraction level of the antagonistic muscle pair.**

***Keywords*—Electromyography, Tele-Impedance, Rehabilitation Robotics, Hand Stiffness**

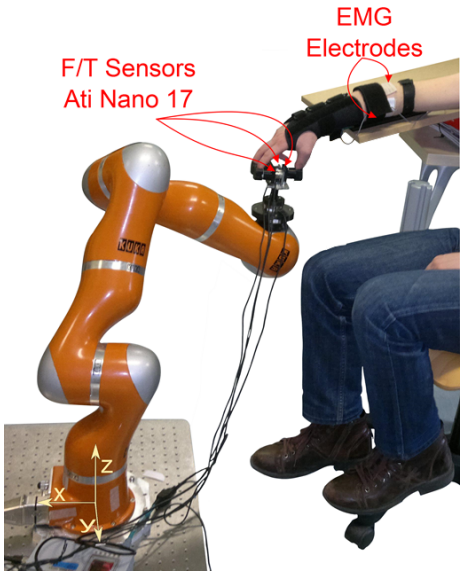

Fig. 1: Experimental setup used for the trials. The KUKA applies planar perturbations to the fingers of the subject and the resulting forces are measured at the fingertips along with the surface EMG signals from the FDS and EDC muscles.

I. Introduction

The need for accurate reproduction of human hand and arm functionalities ranges across many disciplines of robotics, including rehabilitation robotics and prosthetics and teleoperation for surgical or disaster-response robotics. Traditional teleoperation robotics uses direct position control to operate the end-effector, potentially producing undesired interaction forces. Alternatively, force information can be fedback to the operator to result in finer control that may be subject to noticeable lag, resulting in potential stability issues [1], [2]. To address these drawbacks, previous work from our lab devised a method for tele-impedance operation of a compliant slave robot [3], [4]. In tele-impedance, a compound reference command which includes the position and stiffness profiles of the master is replicated by a slave robot in real-time. Several physical interaction scenarios have been investigated to evaluate the efficiency of the proposed framework in establishment of an appropriate mechanical interface between the robot and the uncertain environment [4], [5]. As an extension, the work below presents a pilot study in modelling and real-time tracking of the human finger stiffness for future applications in rehabilitation robotics or other teleoperation scenarios.

Past studies on human stiffness have focused mainly on the arm and found that the endpoint stiffness is influenced both by limb configuration (joint angles and limb segment lengths) [6] and joint torques [7]. Another factor that affects the endpoint stiffness of a limb is antagonist co-contraction. In the hand motor control system, in fact, antagonist co-contraction serves several purposes, including monitoring limb position, especially when learning a new task, decelerating the limb in ballistic movements, and increasing stiffness [8]. Stiffening behavior can be realized to stabilize movement or to fix posture in isometric tasks [9]. Previous work examining finger and hand stiffness has explored various topics including the mechanical impedance of the fingers [10] or at the fingertip [11], pinch grasp stiffness during an isometric grasp task [12], or variance of stiffness depending on finger force or posture [13]. The estimation of the impedance parameters in these studies is mainly achieved by an off-line post-processing phase, imposing severe limitations in real-time applications such as

Authors are with Department of Advanced Robotics (ADVR), Istituto Italiano di Tecnologia, Via Morego 30, 16163 Genova, Italy. M. Rossi, A. Altobelli, A. Ajoudani and A. Bicchi are also with the Centro di Ricerca "E. Piaggio", Università di Pisa, Largo L. Lazzarino 1, 56122 Pisa, Italy. E-mails: {matteo.rossi, alessandro.altobelli, sasha.godfrey, arash.ajoudani, antonio.bicchi}@iit.it.

tele-impedance control of the prosthetic or robotic hands. At first, this might imply that a complete model and thus control of the finger motion and stiffness trajectories are required to perform a target manipulation task. However, observations in human control suggest that the entral nervous system solves for this complexity in an elegant and coordinated manner which has been well-recognized with the concept of hand synergies [14], [15], [16]. While the exploitation of this concept in kinematic coordinates has lead to the development of several simple, effective and adaptive robotic designs and control strategies (e.g. see [16], [17]), its extension to dynamic coordinates, such as coordinated stiffening of the fingers, remains to be investigated.

Toward the twofold purpose of investigating the presence of coordinated regulations of the finger stiffness in human hand and the establishment of a real-time technique in modelling and identification of the finger stiffness while grasping, we explore the relationship between the fingertip stiffness and the EMG activity of the antagonist muscles contributing to this profile. To achieve this, the experiments are performed using a tripod-grasp device developed in the lab that contains a 6-DOF force/torque sensor at each contact point (thumb, index, and middle fingers) as well as a global 6-DOF force/torque sensor in the base of the device. While constrained in a tripod posture in the Tripod Device, subjects were asked to hold a stable level of stiffness without applying grasping forces and experienced a series of perturbations provided by the KUKA lightweight robot arm. EMG was recorded alongside force/torque measurements. Consequently, we established the mapping between the fingertip stiffness profiles, as calculated from the force/torque measurements, and the EMG data.

II. Materials and Methods

A. Study Design

Five subjects participated in the experiment, 3 males and 2 females aged 28 $\pm$ 3 years. Before participating, subjects signed an informed consent form approved by the local ethical committee. Subjects placed their fingers in a Tripod Device and maintained a steady level of hand stiffness, as measured by surface EMG, while experiencing perturbations provided by the KUKA lightweight robot (Figure 1). Subjects completed the first trial while relaxed and then increased stiffness to low, medium, and finally high levels in subsequent trials. The block of four trials was repeated three times for a total of 12 trials. Each perturbation trial lasted 35 seconds and the experiment lasted less than an hour.

B. Tripod Device and Experimental Setup

The Tripod Device is an instrumented manipulandum that can be grasped with three fingers and includes three individual contact surfaces. Each contact surface consists of a contact module rigidly attached to the structure of the manipulandum, through an interface engineered in Acrilonitrile-Butadiene-Stirene (ABS) rapid prototyping material. Every contact module consists of a cylindrical base in ABS (rigid case, Young Modulus 1.4 GPa). To minimize structural deformations, the core frame of the Tripod Device was built in aluminium using a CNC (Computer Numerical Control) machine.

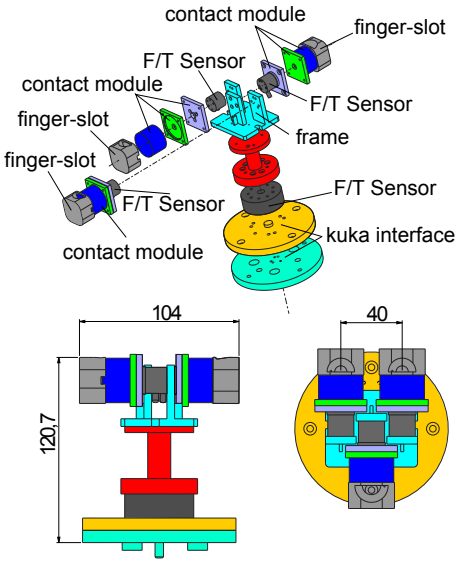

Fig. 2: Exploded drawing view of the Tripod Device and its main features with dimensions in [mm].

A force/torque sensor (Series Nano 17 by ATI, Apex, NC, USA) was positioned below the interface where each contact module was attached to measure the force and torque components applied by each finger. A finger-slot was designed and fixed to each contact surface to minimize the relative movements between the finger and the Tripod Device. A fourth F/T sensor (Series Nano 45 by ATI, Apex, NC, USA) placed at the base of the structure provided an independent measure of the external wrench. An exploded drawing view of the manipulandum with dimensions is reported in Fig. 2.

The Tripod Device was mounted on the end-effector of a 7-DOF robot arm: the KUKA lightweight robot (KUKA/DLR). All force and displacement measures were reported in the base reference frame of the KUKA. The KUKA, which has a positioning repeatability of $\pm 0.05mm$, was programmed to follow a planar random trajectory, keeping constant the orientation angles of the end-effector (roll, pitch, yaw), so that the Tripod Device remained parallel to the ground and maintained the same orientation with respect to the fixed frame (Figure 1). The subjects adopted a tripod posture and inserted the index finger, the middle finger, and the thumb in the dedicated finger-slots of the Tripod Device. At each finger, the forces in response to the position perturbation were measured by the contact point F/T sensors described above. Surface EMG signals on the forearm were measured and amplified with a Delsys-Bagnoli 16 (Delsys Inc.). The data acquisition and synchronization interface between the KUKA controller, the four F/T sensors, and the EMG acquisition board were developed in Microsoft Visual C++ environment.

C. Protocol

Subjects were seated for the duration of the experiment. Surface EMG electrodes were placed on the flexor digitorum superficialis (FDS) and extensor digitorum communis (EDC)

muscles. To minimize cross-talk from neighboring muscles, the electrodes were positioned following the methods described by Perrotto et al. [18].

Each subject placed his thumb, index, and middle fingertips in the finger-slots of the Tripod Device; his arm was immobilized against a board at an angle to allow the tripod grasp to be comfortably maintained parallel to the ground, see Fig. 1. In a pre-trial, the KUKA did not perturb the subject, and the subject was instructed to produce maximum hand stiffness without applying any force to the F/T sensors. The level of co-contraction produced in this trial was used as an upper-bound for the co-contraction level in subsequent trials. In the first trial, the subject remained relaxed while the KUKA perturbed the subject following the trajectory described above. In subsequent trials, while the KUKA perturbed the hand, subjects were asked to produce respectively a "low", "medium" and "high" level of stiffness without squeezing the Tripod Device; to help them maintaining constant and coherent co-contraction levels, subjects were provided visual feedback on the co-contraction level and the visualized targets for the three conditions corresponded roughly to 20, 40, or 60% of the maximum level of co-contraction previously obtained. Subjects were also instructed to prioritize stability of co-contraction level over accuracy of targeted level; that is, subjects aimed to keep a low standard deviation over producing a particular mean co-contraction level. The block of four trials was repeated three times for a total of 12 trials.

D. Data Analysis

To estimate the endpoint stiffness at each of the three fingers, we adopted the same techniques used in [4] for the arm. Following Perrault et al. [19] we applied continuous stochastic perturbations for 35 seconds to the subject's fingers through the Tripod Device. The perturbations were applied in x and y directions, with a peak-to-peak value of 10 mm in each direction and with a frequency spectrum that was flat in the range of 0 to 6Hz and null elsewhere. The first 5 seconds of data were discarded to allow the subject to reach the required stiffness level.

For each finger, the multiple-input, multiple-output (MIMO) dynamics of the endpoint stiffness were decomposed into four linear single-input, single output (SISO) subsystems; the identification of each SISO subsystem was performed in the frequency domain using a nonparametric algorithm [20]. The endpoint inertia, viscosity and stiffness matrices, I, B and K, where found by comparing each SISO transfer function with a second order linear model of the type:

$$G_{i,j}(s) = I_{i,j}s + B_{i,j}s + K_{i,j}s, \quad i,j = x,y.$$

The external wrench measured at the base of the Tripod Device with the ATI Series Nano 45 force/torque sensor was compared with the external wrench derived from the three force-torque sensors placed under the fingers to verify that the measurements were correct. The surface EMG signals were acquired with a Delsys-Bagnoli 16 apparatus, sampled at 750Hz, high-pass filtered at a cut-off frequency of 4 Hz with a 4th order Butterworth filter and then rectified. Finally,

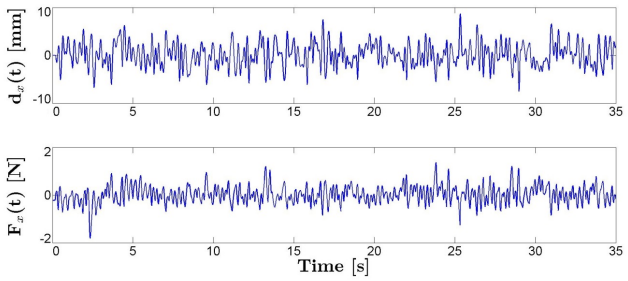

Fig. 3: x components of a typical endpoint displacement $d(t)$ and the resulting force $F(t)$. $F(t)$ and $d(t)$ were used to estimate the endpoint stiffness of the fingers by means of a nonparametric algorithm in the frequency domain [20].

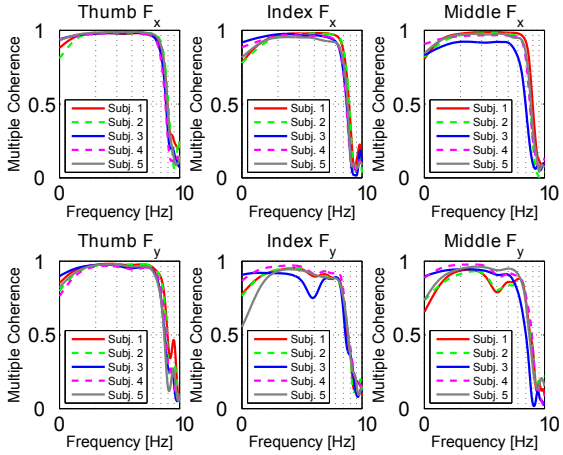

Fig. 4: Example of Multiple Coherence function values for the five subjects.

each rectified signal was low-pass filtered in order to obtain its envelope. The average values of the EMG signals relative to the FDS and EDC muscles, respectively p' and p'', were calculated at each trial. The resulting level of co-contraction (Lcc) was computed as:

$$Lcc_{s,t} = \frac{1}{2}\left(\frac{p'_{s,t}}{p'_{s,\max}} + \frac{p''_{s,t}}{p''_{s,\max}}\right)$$

Where s indicates the subject, t the trial number and $p'_{s,\max}$, $p''_{s,\max}$ the maximum EMG values recorded respectively at channel 1 and channel 2 of subject s.

III. Results

Figure 3 shows the x component of a typical endpoint displacement $d(t)$ along with the x component of the resulting force $F(t)$ measured at the index fingertip. To evaluate the linear dependency of each output (forces) to all system inputs (displacements), the multiple coherence indices were computed on the obtained measurements. A strong linear dependency of the inputs and the outputs was found in the frequency range 0-6 Hz, as shown in the Figure 4; for this

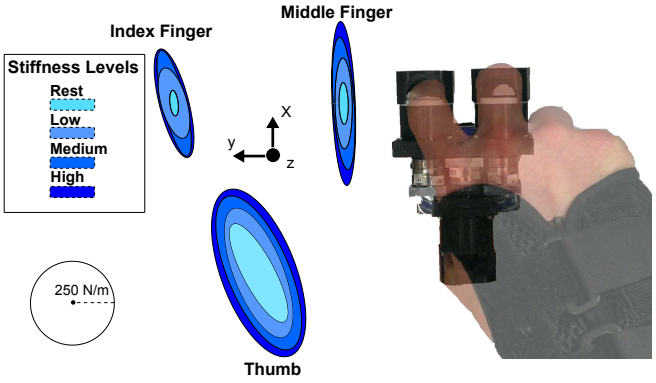

Fig. 5: Endpoint stiffness ellipses generated by Subject 1 during four consecutive trials.

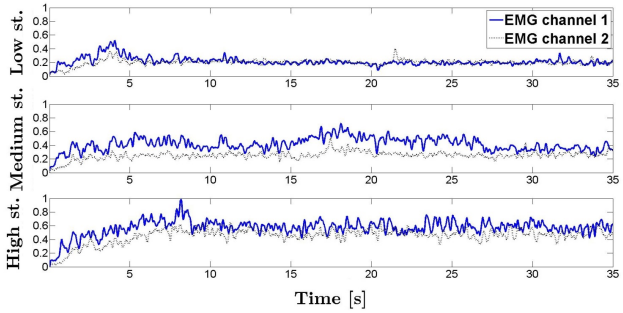

Fig. 6: Typical normalized EMG signals for three different targeted stiffness levels. The data are relative to Subject 2.

reason the parameter estimation was performed in the same range.

After estimating each stiffness matrix K, its symmetric K_s and asymmetric K_a parts were extracted:

$$K_s = \frac{1}{2}(K + K^T) \qquad K_a = \frac{1}{2}(K - K^T)$$

The error of approximation was computed as:

$$e = \frac{||Ka||_2}{||Ks||_2},$$

obtaining a mean value $\bar{e} \approx 0.07$.

The eigenvalues λ_1 and λ_2 (with $\lambda_1 < \lambda_2$) of Ks and the corresponding eigenvectors, $\mathbf{v_1}$ and $\mathbf{v_2}$, were computed. In all of the examined cases, Ks was found to be positive definite, with λ_1 and λ_2 real and greater than 0.

Figure 5 presents the endpoint stiffness ellipses that were generated by one of the subjects during four consecutive trials (with four different indications on the stiffness set-point level). Stiffness ellipses are a consolidated method of representing the endpoint stiffness. In the 2D case, the major and minor axes of the ellipse represent respectively λ_2 and λ_1, while the orientation θ of the ellipse is given by the angle between $\mathbf{v_2}$ and the x axis. As expected, the stiffness ellipse area ($A = \pi\lambda_1\lambda_2$) increases with increasing targeted stiffness levels. On the other hand, the orientation

TABLE I: Average ellipse orientations for the four targeted stiffness levels.

$\theta(^\circ)$	Finger	Rest	Low St.	Medium St.	High St.
Subject 1	*I*	8.1	10.3	0.2	5.7
	M	12.1	14.6	15.5	15.6
	T	10.6	14.0	14.2	19.1
Subject 2	*I*	20.8	22.4	24.1	−15.0
	M	24.8	25.9	32.2	22.8
	T	12.3	1.5	−6.1	0.5
Subject 3	*I*	−1.6	3.1	4.1	4.1
	M	28.2	7.5	2.3	3.2
	T	5.4	11.4	2.5	−2.0
Subject 4	*I*	34.1	8.9	6.7	−11.6
	M	27.3	15.6	20.5	24.7
	T	27.3	23.5	22.0	22.9
Subject 5	*I*	15.3	13.5	15.5	16.7
	M	15.2	18.1	−10.7	−25.7
	T	13.7	20.3	23.3	−10.2

TABLE II: Average ratio $\frac{\lambda_1}{\lambda_2}$ of the ellipse axes for the four targeted stiffness levels.

$\frac{\lambda_1}{\lambda_2}$	Finger	Rest	Low St.	Medium St.	High St.
Subject 1	*I*	0.13	0.09	0.19	0.25
	M	0.27	0.31	0.27	0.23
	T	0.19	0.14	0.16	0.17
Subject 2	*I*	0.41	0.34	0.31	0.30
	M	0.37	0.26	0.22	0.19
	T	0.22	0.17	0.20	0.30
Subject 3	*I*	0.22	0.19	0.17	0.16
	M	0.51	0.29	0.26	0.32
	T	0.48	0.44	0.32	0.20
Subject 4	*I*	0.61	0.43	0.61	0.58
	M	0.07	0.32	0.42	0.40
	T	0.23	0.31	0.40	0.46
Subject 5	*I*	0.14	0.14	0.18	0.21
	M	0.18	0.25	0.33	0.19
	T	0.17	0.23	0.26	0.40

θ, as well as the shape (here quantified with the ratio $\frac{\lambda_1}{\lambda_2}$), of the stiffness ellipse does not appear to be correlated with the targeted stiffness levels. Table I reports the mean values of the stiffness ellipses' orientations corresponding to different targeted stiffness levels. For each subject, the values are distributed in three different rows *I*, *M* and *T* that correspond respectively to the index finger, middle finger and thumb. Following the same structure of Table I, Table II presents the average ratio $\frac{\lambda_1}{\lambda_2}$ with respect to different targeted stiffness levels.

To further investigate the behavior of the stiffness components λ_1 and λ_2 at each finger, we used the measured surface EMG signals from the FDS (channel 1) and EDC (channel 2) muscles as an indicator of the global stiffness of the hand. Figure 6 shows the filtered EMG signals acquired from one of the subjects during three different trials. The three trials corresponded to three increasing targeted stiffness levels. Each signal was normalized to the maximum value produced by the subject during the pre-trial phase for the

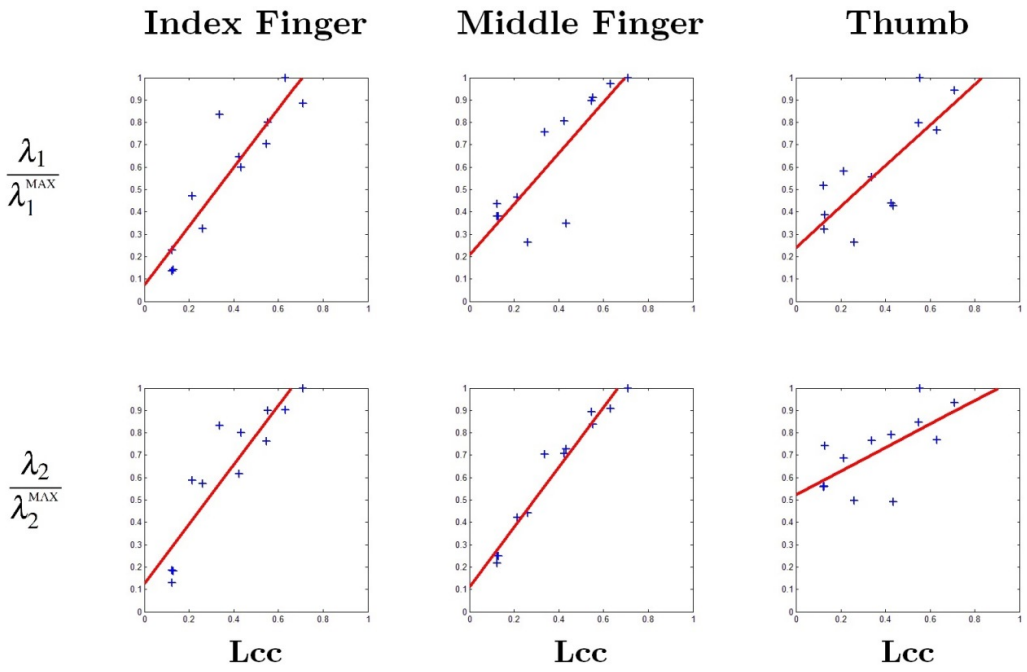

Fig. 7: Linear regression of normalized stiffness axes with respect to the level of co-contraction (*Lcc*). The graphs are relative to Subject 3.

TABLE III: Angular coefficients $m_{i,f}$ of the fitting lines along with the average coefficient of determination R^2 for each subject.

	$m_{1,I}$	$m_{2,I}$	$m_{1,M}$	$m_{2,M}$	$m_{1,T}$	$m_{2,T}$	R^2
*Subject*1	1.20	1.25	1.13	1.17	1.25	0.71	0.73
*Subject*2	1.19	1.18	0.93	0.96	1.11	0.61	0.86
*Subject*3	1.31	1.33	1.14	1.34	0.91	0.53	0.72
*Subject*4	0.88	0.74	0.45	0.67	0.70	0.50	0.42
*Subject*5	1.68	2.60	2.13	1.67	1.95	1.13	0.60

corresponding EMG channel.

The acquired EMG signals were used to compute the level of co-contraction (*Lcc*) index for each trial. To measure the correlation between the stiffness components at each finger and the *Lcc* index, Pearson's Correlation Coefficient (PCC) was used. PCC produces a measure of the linear correlation between two measures; it can range from -1 (total negative correlation) to 1 (total positive correlation), with 0 indicating absence of correlation. The average correlation coefficient obtained between λ and *Lcc* was:

$$\overline{PCC} \approx 0.81$$

For every subject, we then linearly fitted the normalized values of λ_1 and λ_2 with respect to *Lcc*. A total of six fittings were performed for each subject (two per finger) by implementing least-squares regression to find the coefficients $m_{i,f}$ and $q_{i,f}$ in the following equation:

$$\frac{\lambda_{i,f}}{\lambda_{i,f}^{MAX}} \approx m_{i,f} Lcc + q_{i,f} \qquad i = 1,2$$

where $f = T, I, M$ indicates thumb, index or middle finger, respectively, and $\lambda_{i,f}^{MAX}$ is the maximum value of $\lambda_{i,f}$ among the 12 trials. The results for one of the subjects are presented in Figure 7. The slopes of the fitting lines for each subject along with the mean coefficient of determination R^2 are given in Table III.

IV. Discussion

The experimental results corroborate the feasibility of a generalized mapping between the EMGs recorded from the forearm and the hand stiffness.

Since the aim of this work was not the generation of an accurate model of hand stiffness control but instead to move a step towards the design of more natural and better performing control interfaces for hand prostheses and teleoperation, we focused only on the relationship between the hand stiffness and the FDS and EDC muscles. In particular, we represented the endpoint stiffness of the fingers with stiffness ellipses and found that their area increased with respect to increasing levels of co-contraction *Lcc*, while their orientation and shape did not seem to be related to *Lcc*. In fact, the variation of θ and $\frac{\lambda_1}{\lambda_2}$ across trials as seen in Table I and II does not appear to depend on the requested stiffness level; this conjecture is supported by the studies on the human limb stiffness, which state that the orientation and shape of the endpoint stiffness ellipses is mainly determined by posture [21].

In general, the endpoint stiffness of the thumb, index and middle fingers was found to increase when the level of co-contraction *Lcc* increased. Furthermore, the results of the linear fittings (Table III) show that, not only the relationship between stiffness and *Lcc* was nearly linear, but also that, with the exception of $m_{2,T}$, the slopes of the fitting lines tended to maintain a similar value within the same

subject. This result is very important because it highlights a tendency of the fingers to stiffen in a coordinated way that is also proportional to the level of co-contraction of the EDC and FDS muscles. However, in order to produce a simple but efficient generalized mapping between hand stiffness and co-contraction, further studies should be conducted. In particular, in this work we focused on the relationship between co-contraction and hand stiffness in absence of grip force. The subjects were in fact asked not to produce any grip force and, by checking the force/torque measurements, we found that the request was fulfilled in all the trials with the exception of Subject 4 and Subject 5 during the high stiffness condition. This simplification was made in order to better understand the role of co-contraction in the control of hand stiffness, but we believe that the mapping will not be applicable in real tasks unless it will also take into account the possibility of the exertion of grip forces.

V. Conclusions

We have presented an approach for the characterization and mapping of the hand stiffness. To the best of our knowledge, this is the first work that analyses the relationship between co-contraction of the FDS and EDC muscles and the endpoint stiffness of thumb, index and middle finger; the results suggest that, while the shape and orientation of the stiffness ellipses are mainly influenced by the hand posture, there is a nearly linear relationship between the level of co-contraction and the length of the ellipses' axes. Furthermore, by normalizing the endpoint stiffness components of each finger, we were able to identify a rate of growth between the stiffness components and the level of co-contraction that had little variations among different fingers of the same subject. These results show the feasibility of a generalized mapping between the EMGs recorded from the FDS and EDC muscles and the hand stiffness. Such a mapping could be applied to many disciplines of robotics; in particular, it could allow the design of more natural and efficient control schemes for upper limb prostheses.

Acknowledgment

This work is supported in part by the European Research Council under the Advanced Grant SoftHands "A Theory of Soft Synergies for a New Generation of Artificial Hands" no. ERC-291166 and under the EU FP7 project WEARHAP "WEARable HAPtics for Humans and Robots" no. 601165.

References

[1] B. Hannaford, "A design framework for teleoperators with kinaesthetic feedback," *IEEE Transactions on Robotics and Automation*, vol. 5, no. 4, pp. 426–434, 1989.

[2] T. Imaida, Y. Yokokohji, M. O. T. Doi, and T. Yoshikawa, "Ground space bilateral teleoperation of ETS-VII robot arm by direct bilateral coupling under 7-s time delay condition," *IEEE Transactions on Robotics and Automation*, vol. 20, no. 3, pp. 499–511, 2004.

[3] A. Ajoudani, N. Tsagarakis, and A. Bicchi, "Tele-impedance: Towards transferring human impedance regulation skills to robots," in *International Conference of Robotics and Automation - ICRA 2012*, Saint Paul, MN, USA, May 14 - 18 2012, http://www.youtube.com/watch?v=-Fn2dObnFpw.

[4] A. Ajoudani, N. G. Tsagarakis, and A. Bicchi, "Tele-Impedance: Teleoperation with impedance regulation using a body-machine interface," *International Journal of Robotics Research*, vol. 31(13), pp. 1642–1655, 2012, http://www.youtube.com/watch?v=KPO6IO7Tr-Q.

[5] N. Karavas, A. Ajoudani, N. Tsagarakis, J. Saglia, A. Bicchi, and D. Caldwell, "Tele-impedance based assistive control for a compliant knee exoskeleton," *Robotics and Autonomous Systems*, 2014.

[6] F. A. Mussa-Ivaldi, N. Hogan, and E. Bizzi, "Neural, mechanical, and geometric factors subserving arm posture in humans," *The Journal of neuroscience*, vol. 5, no. 10, pp. 2732–2743, 1985.

[7] S. C. Cannon and G. I. Zahalak, "The mechanical behavior of active human skeletal muscle in small oscillations," *Journal of Biomechanics*, vol. 15, no. 2, pp. 111–121, 1982.

[8] A. M. Smith, "The coactivation of antagonist muscles," *Canadian journal of physiology and pharmacology*, vol. 59, no. 7, pp. 733–747, 1981.

[9] D. R. Humphrey and D. J. Reed, "Separate cortical systems for control of joint movement and joint stiffness: reciprocal activation and coactivation of antagonist muscles," *Adv Neurol*, vol. 39, pp. 347–372, 1983.

[10] A. E. Fiorilla, F. Nori, L. Masia, and G. Sandini, "Finger impedance evaluation by means of hand exoskeleton," *Annals of biomedical engineering*, vol. 39, no. 12, pp. 2945–2954, 2011.

[11] A. Z. Hajian and R. D. Howe, "Identification of the mechanical impedance at the human finger tip," *Journal of biomechanical engineering*, vol. 119, no. 1, pp. 109–114, 1997.

[12] H. Hoppner, D. Lakatos, H. Urbanek, C. Castellini, and P. van der Smagt, "The grasp perturbator: Calibrating human grasp stiffness during a graded force task," in *Robotics and Automation (ICRA), 2011 IEEE International Conference on*. IEEE, 2011, pp. 3312–3316.

[13] T. E. Milner and D. W. Franklin, "Characterization of multijoint finger stiffness: dependence on finger posture and force direction," *Biomedical Engineering, IEEE Transactions on*, vol. 45, no. 11, pp. 1363–1375, 1998.

[14] M. Turvey, "Action and perception at the level of synergies," *Human Movement Science*, vol. 26, no. 4, pp. 657–697, 2007.

[15] M. Santello, M. Flanders, and J. Soechting, "Postural hand synergies for tool use," *The Journal of Neuroscience*, vol. 18, no. 23, pp. 10 105–10 115, 1998.

[16] A. Bicchi, M. Gabiccini, and M. Santello, "Modelling natural and artificial hands with synergies," *Philosophical Transactions of the Royal Society B: Biological Sciences*, vol. 366, no. 1581, pp. 3153–3161, 2011.

[17] M. G. Catalano, G. Grioli, A. Serio, E. Farnioli, C. Piazza, and A. Bicchi, "Adaptive synergies for a humanoid robot hand," in *Humanoid Robots (Humanoids), 2012 12th IEEE-RAS International Conference on*. IEEE, 2012, pp. 7–14.

[18] A. Perotto and E. F. Delagi, *Anatomical guide for the electromyographer: the limbs and trunk*. Charles C Thomas Publisher, 2005.

[19] E. J. Perreault, R. F. Kirsch, and P. E. Crago, "Multijoint dynamics and postural stability of the human arm," *Experimental brain research*, vol. 157, no. 4, pp. 507–517, 2004.

[20] E. J. Perreault, R. F. Kirsch, and A. M. Acosta, "Multiple-input, multiple-output system identification for characterization of limb stiffness dynamics," *Biological cybernetics*, vol. 80, no. 5, pp. 327–337, 1999.

[21] D. Shin, J. Kim, and Y. Koike, "A myokinetic arm model for estimating joint torque and stiffness from emg signals during maintained posture," *Journal of neurophysiology*, vol. 101, no. 1, pp. 387–401, 2009.